JACS
JOURNAL OF THE AMERICAN CHEMICAL SOCIETY
Article
pubs.acs.org/JACS

Elucidation of the Selectivity of Proton-Dependent Electrocatalytic CO_2 Reduction by *fac*-Re(bpy)$(CO)_3$Cl

John A. Keith,[†] Kyle A. Grice,[§] Clifford P. Kubiak,[§] and Emily A. Carter*[,†,‡,⊥]

[†]Department of Mechanical and Aerospace Engineering and [‡]Program in Applied and Computational Mathematics and [⊥]Andlinger Center for Energy and the Environment, Princeton University, Princeton, New Jersey 08544-5263, United States

[§]Department of Chemistry and Biochemistry, University of California, San Diego, 9500 Gilman Drive, Mail Code 0358, La Jolla, California 92093-0358, United States

Supporting Information

ABSTRACT: A complete mechanism for the proton-dependent electrocatalytic reduction of CO_2 to CO by *fac*-Re(bpy)$(CO)_3$Cl that is consistent with experimental observations has been developed using first principles quantum chemistry. Calculated one-electron reduction potentials, nonaqueous pK_a's, reaction free energies, and reaction barrier heights provide deep insight into the complex mechanism for CO_2 reduction as well as the origin of selectivity for this catalyst. Protonation and then reduction of a metastable Re−CO_2 intermediate anion precedes Brønsted-acid-catalyzed C−O cleavage and then rapid release of CO at negative applied potentials. Conceptually understanding the mechanism of this rapid catalytic process provides a useful blueprint for future work in artificial photosynthesis.

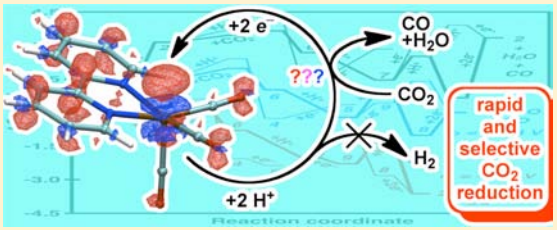

INTRODUCTION

CO_2 reduction is of immediate concern, not only as a means to reduce atmospheric CO_2 but also as a potentially sustainable source of renewable fuels and commodity chemicals. Efforts are being devoted to couple CO_2 reduction, water oxidation, and solar energy in artificial photosynthetic systems. Deploying large-scale artificial photosynthetic devices in turn requires developing catalysts that favor proton-dependent CO_2 reduction over proton reduction to hydrogen. CO_2 reductions that selectively produce liquid fuels are preferred,[1,2] but efficient CO_2 reduction to CO would also be useful for generating syngas to synthesize methanol or Fischer−Tropsch fuels.

A variety of homogeneous catalysts have been studied for electrocatalytic CO_2 reduction.[3−6] Of particular promise are *fac*-Re(bpy-R)$(CO)_3$X complexes (bpy-R = 4,4′-disubstituted-2,2′-bipyridine; X = anionic ligand or solvent with counter-anion) originally reported by Lehn and co-workers.[7] (Since all five- and six-coordinate Re complexes reported in this study are *fac*-, this label will henceforth be omitted.) These electrocatalysts reduce CO_2 to CO with extremely high Faradaic efficiency, even in the presence of excess water. Studies have shown that at least two operational CO_2 reduction mechanisms lead to CO: (1) a relatively slow one-electron pathway and (2) a more rapid two-electron pathway.[8]

The one-electron process is characterized by CO_2 reductive disproportionation to CO and CO_3^{2-} at the first reduction of Re(bpy-R)$(CO)_3$X. Cyclic voltammetry experiments display no current enhancement at the first reduction, indicating a very slow process. Photochemical CO_2 reduction by Re(bpy)-$(CO)_3$X likely follows a similar mechanism[9,10] and also has sluggish kinetics, yielding only 5−12 turnovers per hour.[11]

The two-electron pathway, by contrast, displays an unacceptably high overpotential for practical applications, but it also displays much more rapid kinetics on the order of tens to hundreds of turnovers per second. (The high overpotential can also be ameliorated, in principle with semiconductor electrodes and synthetic modification of the ligand backbone.)[12,13] This process appears to be activated by two separate one-electron reductions starting from Re(bpy-R)$(CO)_3$X complexes (R = 4,4′-(H or *t*Bu)-2,2′-bipyridine).[14] Unlike the one-electron process, this reaction is proton-dependent, as evidenced by significantly more rapid catalysis in the presence of higher concentrations of Brønsted acids.[13,15] The Re(bpy-*t*Bu)$(CO)_3$X catalyst is even more active than the Re(bpy-H)$(CO)_3$X catalyst.[14] X-ray crystal structures of several of the reactive $[Re(bpy\text{-}R)(CO)_3]^{-1}$ anions have been obtained,[13,16,17] but despite the significant advances in understanding this catalyst, many details about its two-electron CO_2 reduction mechanism remain elusive (Scheme 1), inhibiting design of other catalysts with rapid kinetics but lower overpotentials. A recent experimental and theoretical study showed that the non-innocent bpy ligand affects the electronic structure of the $[Re(bpy)(CO)_3]^-$ anion by causing the Re center to formally take on a Re^0 state while storing the extra electron.[18] The delocalized electronic state helps explain the origin of this catalyst's selectivity, but the origin of its observed proton dependence and a detailed mechanistic picture that pinpoints its electrocatalytic rate-determining step (needed to rationally design better catalysts) have been unknown until now.

Received: June 25, 2013
Published: September 20, 2013

dx.doi.org/10.1021/ja406456g | J. Am. Chem. Soc. 2013, 135, 15823−15829

Scheme 1. The Proton-Dependent Electrocatalytic Reduction of CO_2 to CO by $Re(bpy)(CO)_3Cl$

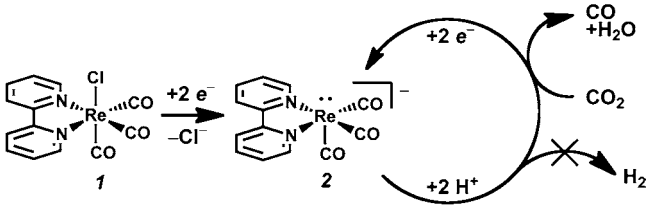

We report first principles quantum chemistry studies of CO_2 reduction by $Re(bpy)(CO)_3Cl$ in acetonitrile with added proton sources. We use calculated reduction potentials, pK_a values, reaction free energies, and activation barriers to provide deep understanding of the mechanism. Similar theoretical approaches have been used recently to examine homogeneous hydrogen evolution[19,20] as well as pyridinium-catalyzed electroreduction of CO_2 to methanol,[21−24] originally reported by Bocarsly and co-workers.[25,26] This work opens the door for accelerated development of new generations of highly active catalysts for CO_2 reduction, which in turn can lead to advanced artificial photosynthesis systems.

COMPUTATIONAL METHODS

All theoretical data were obtained from density functional theory (DFT) calculations using the (U)B3LYP[27,28] exchange−correlation functional, performed within the GAMESS-US program.[29,30] Geometries were optimized using 6-31+G** basis sets[31,32] on all atoms except for K and Re, which were represented by LANL2DZ effective core potentials (ECPs) and their corresponding basis sets.[33] 10 and 60 core electrons from K and Re, respectively, were subsumed into the ECPs. Vibrational frequency calculations confirmed the identity of stable intermediates and transition states, and the latter were further validated by intrinsic reaction coordinate calculations. The thermodynamic energy contributions were calculated at the true minimum energy stationary points of the smaller bases using the harmonic oscillator, ideal gas, and rigid rotor approximations.[34] Electronic energies for the optimized structures were then calculated using the larger aug-cc-pVDZ basis sets[35] on all atoms except for K and Re, where the LANL2DZ ECP and basis set were again used on K, while the LANL2DZ ECP and the fully uncontracted basis set were used on Re. Electrostatic solvation energies (from geometries optimized with the continuum solvation model) were obtained using a CPCM[36] implicit solvation model for acetonitrile (ε = 35.69, probe radius = 2.18 Å) with the same basis sets and ECPs as those used to compute the electronic energies. Cl^- and K^+ solvation energies were obtained this way; our rationale for using these energies is given in the Supporting Information. For pK_a calculations, we used a calculation scheme similar to what we employed for pyridinium and pyridinyl radicals,[21,37] except here we used a different explicit proton solvation energy (−260.2 kcal/mol,[38] since these reactions are in acetonitrile) and no explicit solvent molecules in our solvation energies (since these complexes are relatively large and quite capably treated with the solvation model alone). Our pK_a calculations reproduced qualitative trends for measured acidities of acids and bases in acetonitrile, and applying a linear correction to CPCM solvation energy differences (similar to those done in ref 39) yielded pK_as accurate to within 0.8 pK_a units (see Supporting Information). Corrected pK_a data are the ones discussed in the text.

We also compared experimentally determined reduction potentials to calculated standard reduction potentials, taking the absolute potential of the saturated calomel electrode (SCE) in acetonitrile to be −4.422 V.[40] Note that all reduction potentials reported in this work are referenced to the SCE (see Supporting Information). Energy contributions due to an applied electrode potential, ϕ, were modeled by adding $-e\phi$ to all species following each electrochemical reduction step.[41,42]

RESULTS AND DISCUSSION

Bimetallic species are not observed in the electrochemistry during catalysis and are only observed in the absence of substrate. Furthermore, we know from electrochemical kinetics that the catalysis in the presence of CO_2 and acids is first order in Re.[15] Thus, we considered one-electron reduction potentials ($E°$) starting from $Re(bpy)(CO)_3Cl$ (**1**) that result in $[Re(bpy)(CO)_3]^{-1}$ (**2**). Both **1** and **2** have been spectroscopically and structurally characterized.[16] Our theoretical results show closest agreement to experiment when assuming that the first reduction is **1** + e^- → $[Re(bpy)(CO)_3Cl]^{-1}$ (**3**) (calculated $E°$ = −1.50 V, experimental $E°$ = −1.34 V[14]) followed by **3** + e^- → **2** + Cl^- (calculated $E°$ = −1.68 V, experimental $E°$ = −1.73 V[14]). We also considered the reduction of **1** + e^- → $[Re(bpy)(CO)_3]^0$ + Cl^- (calculated $E°$ = −1.92 V) as well as **3** + e^- → $[Re(bpy)(CO)_3Cl]^{2-}$ (calculated $E°$ = −2.39 V), but both potentials are too negative compared with those observed in experiment. The one-electron process leading to $[Re(bpy)(CO)_3]^0$ is less negative (−1.66 V) if an explicit acetonitrile molecule bound to the vacant site of the $[Re(bpy)(CO)_3]^0$ species is considered, yielding an octahedral complex (similar to the complex proposed by Muckerman and Fujita with an explicit THF molecule).[43] Although the $[Re(bpy)(CO)_3]^0$ complex is more stable with an explicit acetonitrile molecule bound to it, complex **2** is not stabilized by an explicit solvent molecule (as was seen spectroscopically in ref 14 and analogous to what was also found in ref 43). The deviations from experiment reduce substantially when considering an explicit counterion (here, modeled as a lone K^+ counterion near the Cl^- ligands in **1** and **3** or the Re vacant site in **2**; see Supporting Information). The calculated $E°$ for $[\mathbf{1}{-}K]^+$ + e^- → **3**-K = −1.41 V, while the calculated $E°$ for **3**-K + e^- → **2**-K + Cl^- = −1.74 V. An added K^+ counterion also does not substantially alter the alternative one-electron processes that form $[Re(bpy)(CO)_3{\cdots}K]^+$ or $[Re(bpy)(CO)_3Cl{\cdots}K]^-$ intermediates, with their calculated standard reduction potentials still not in line with the observed reduction potentials.

Although this study reports model reaction mechanisms for experiments that do not necessarily involve K^+, the substantial improvement in calculated reduction potentials compared with experiment suggests that K^+ is a reasonable model for the actual noncoordinating counterion that reaction intermediates encounter in the electrolyte (e.g., 0.1 M Bu_4N^+). Furthermore, we found that several transition states could not be characterized unless a counterion was allowed to participate in the reaction (*vide infra*).

For completeness, we considered reduction potentials and thermodynamic reaction energies and barrier heights without and with an explicit K^+ cation interacting with any species with at least local anionic character. In general, thermodynamic data without the explicit cation are not qualitatively different. pK_as are reported in pK_a units, and species involved in pK_a calculations do not involve the K^+ counterion since our benchmarking calculations did not consider K^+ counterions (see Supporting Information). Methanol was used as the acid in this current study; discussion about the effects of varying Brønsted acidities will be discussed in future work.

The entire proposed mechanism is presented in Scheme 2. Under experimental conditions, **2** could react with protons to

dx.doi.org/10.1021/ja406456g | J. Am. Chem. Soc. 2013, 135, 15823−15829

Scheme 2. Calculated Electrocatalytic Cycle Consistent with Experimental Observations[a]

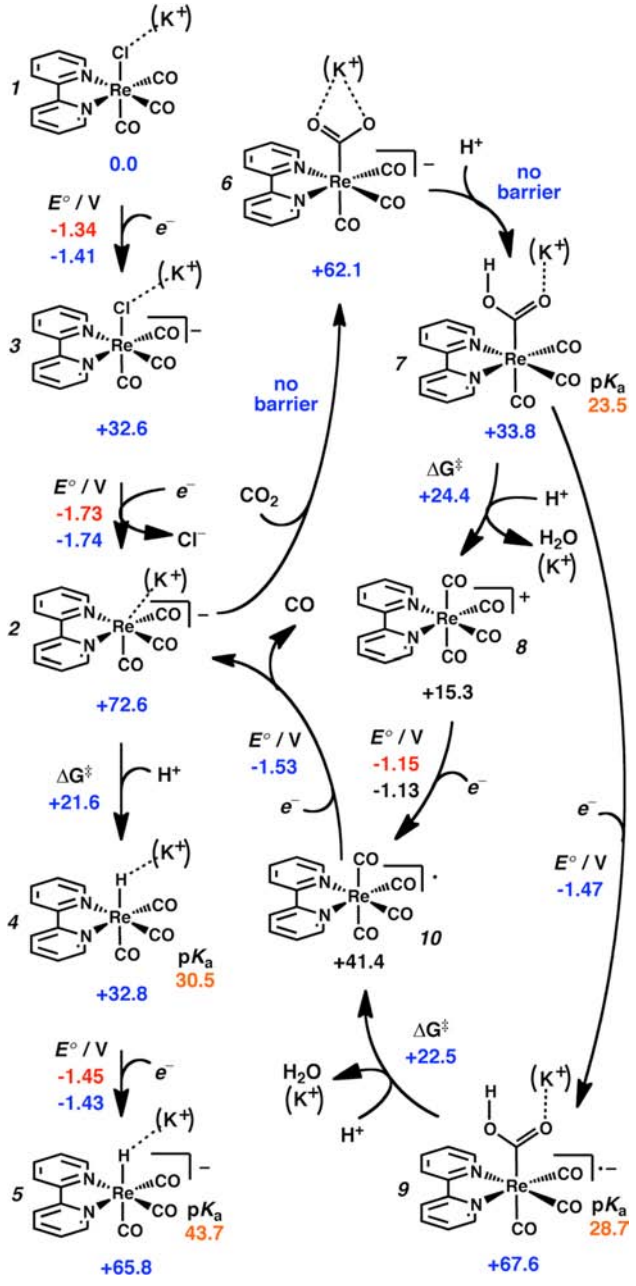

[a]Reaction free energies (labeled below each complex and referenced to complex **1**-K) and barrier heights ($\Delta G^{\ddagger}$) are reported in kcal/mol. Data colors: red = experimentally obtained reduction potentials; black = calculated data with no counterion present; blue = calculated data involving an explicit K^+ counterion interacting with the Re complex; orange = calculated pK_as obtained after applying a linear correction to reduce systematic errors in acetonitrile pK_as (similar to that done in ref 39.). See main text for descriptions about transition states. A comparison of data with and without the explicit counterion can be found in the Supporting Information.

form $[Re(bpy)(CO)_3H]$ (**4**), which in turn could accept an electron and be reduced to $[Re(bpy)(CO)_3H]^-$ (**5**). Either **4** or **5** would be feasible intermediates for H_2 formation. Alternatively, **2** could also react with CO_2 in order to form $[Re(bpy)(CO)_3(CO_2)]^-$ (**6**). We find that complex **6** is unstable in gas phase but is stable in the presence of a counterion and/or when solvated within a continuum solvation model. Complex **6** can then accept a proton from the electrolyte to form $[Re(bpy)(CO)_3(CO_2H)]$ (**7**).

Identifying the cause for this reaction's selectivity is a matter of distinguishing the relative stabilities of complexes **4** and **7** as well as the mechanistic pathways to each species from **2**. A pathway favoring the formation of **4** would result in undesirable H_2 formation. Although this catalytic system is known to be highly selective for CO_2 reduction to CO, our calculations imply that **4** is 1.0 kcal/mol more stable than **7**. Furthermore, the calculated pK_as for **4** and **7** are 30.5 and 23.5, indicating that **2** has a significantly higher affinity for protons than **6**. Although it is known from stopped-flow experiments that $[Re(bpy)(CO)_3]^-$ reacts faster with CO_2 than with weak acids,[13] this catalyst may slightly thermodynamically favor H_2 formation over CO_2 reduction to CO.

The electronic structure of this catalyst was recently reported in a collaborative study utilizing IR spectroscopy, X-ray absorption spectroscopy, and first principles quantum chemistry.[18] In that study, we showed that the HOMO for the ground state structure of **2** was delocalized across both the Re metal center and the bpy π-system (Figure 1a). One might then expect that this HOMO more easily interacts with the CO_2 π^*

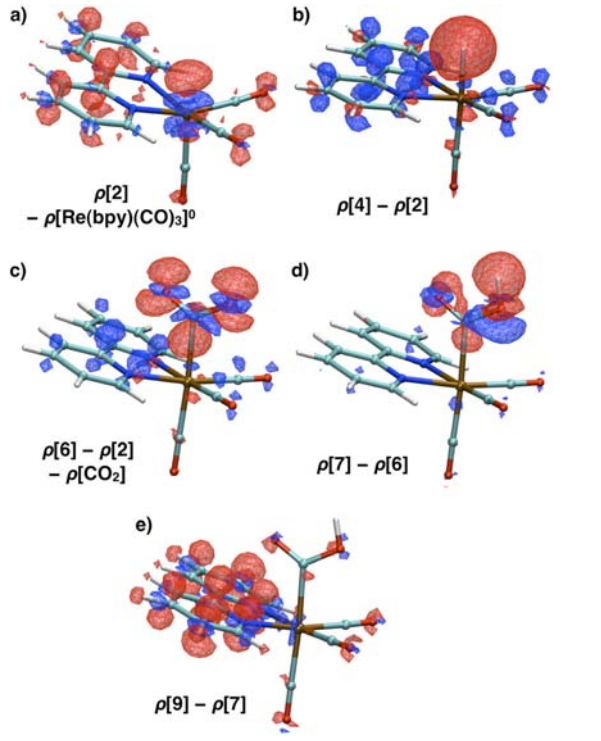

Figure 1. Electron density difference plots depicting intramolecular charge redistribution (red = increased density; blue = decreased density) caused by (a) adding an electron to $[Re(bpy)(CO)_3]^0$ to identify the HOMO of $[Re(bpy)(CO)_3]^-$, (b) adding H^+ to $[Re(bpy)(CO)_3]^-$, (c) adding CO_2 to $[Re(bpy)(CO)_3]^-$, (d) adding H^+ to $[Re(bpy)(CO)_3(CO_2)]^-$, and (e) adding an electron to $[Re(bpy)(CO)_3(CO_2H)]$ to identify the HOMO of $[Re(bpy)(CO)_3(CO_2H)]^-$. Isosurfaces depict density differences plotted with a 0.005 isovalue. Figures made using VMD.[45] Note the delocalized HOMO in panel a is coincidentally similar to the HOMO orbital diagrams in ref 43 even though HOMO orbitals generated directly from single-determinant Kohn–Sham DFT calculations are not unique.

dx.doi.org/10.1021/ja406456g | J. Am. Chem. Soc. 2013, 135, 15823–15829

orbitals. To further probe the significance of this hypothesis, we calculated density difference plots (Figure 1) showing the intramolecular charge density polarization resulting from reactions **2** + H^+ → **4**, **2** + CO_2 → **6**, and **6** + H^+ → **7**, as well as the reduction **7** + e^- → **9**.

Figure 1b shows that there is a substantial increase of electron density at the Re−H bond concomitant with a decrease of electron density within the bpy π-system upon protonation of $[Re(bpy)(CO)_3]^-$. Likewise, Figure 1c shows that there is substantial increase of electron density at the Re−C bond and at the O lone pairs of CO_2 (as well as decreased electron density within the bpy π-system) upon reaction of CO_2 with $[Re(bpy)(CO)_3]^-$. In these two cases, electron density has transferred from the bipyridine ligand to the Re−X bond, which results in a slight lengthening of the bridging C−C bond in the bpy group by ∼0.05 Å relative to that for complex **2**. Interestingly, Figure 1d shows that protonating **6** does not result in substantial polarization of the bpy ligand, but Figure 1e shows that an electron added to **7** would reside again primarily on the bpy ligand. Figure 1 shows the essential role played by the bpy ligand to act as a source and sink of electrons during electrocatalysis at sufficiently negative applied potentials. The delocalized electronic state of **2** was inferred from a previous study reporting HOMO orbitals from single-determinant KS-DFT calculations,[43] but such analysis is not well-founded because the KS determinant is invariant to arbitrary unitary transformations (i.e., self-consistent KS-DFT calculations can find optimized orbitals that minimize a molecule's energy, but different linear combinations of the same molecular orbitals will always result in the same energy). Thus, KS orbitals are nonunique. The only definitive way to determine the nature of the HOMO is via density difference plots as used in this work, since KS-DFT densities are uniquely determined.

The rationale for selectivity is most clear when considering reaction barrier heights for these processes. Transition state geometries are shown in Figure 2. The CO_2 addition process, **2** + CO_2 → **6**, brings substantial charge rearrangement (see Figure 1c) and has an energy barrier of +11.5 kcal/mol when the transition state geometry is optimized using continuum solvation. No transition state could be characterized when including the K^+ counterion in this particular calculation, which was not particularly surprising since CO_2 addition in the presence of the counterion is 10.5 kcal/mol downhill in energy while only 0.4 kcal/mol downhill without the counterion. Likewise, no transition state could be identified for the **6** + H^+ → **7** process (with or without the K^+ counterion), likely because this reaction is also very downhill in energy and involves electronic rearrangement localized only at the CO_2 group as shown in Figure 1d. If one considered protonation of **6** to be a barrierless process, the highest reaction barrier for the overall selective CO_2 reduction process **2** → **7** is for CO_2 addition, +11.5 kcal/mol, a barrier that is substantially reduced, perhaps even to zero, by the presence of the counterion. This overall process of **2** + CO_2 → **7** is −36.3 kcal/mol downhill when referenced to the energy of a free proton in acetonitrile.

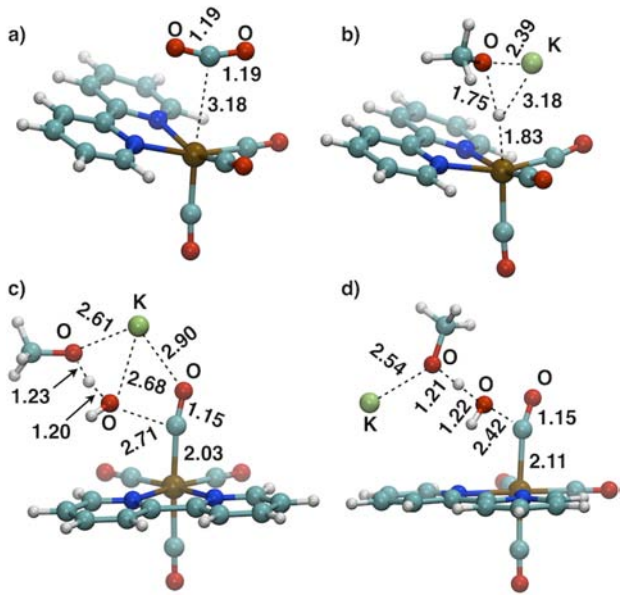

Figure 2. Optimized geometries for transition states for (a) **2** + CO_2 → **6**, (b) **2**-K + MeOH → **4**-K + MeO^-, (c) **7**-K + MeOH → **8** + MeO^- + H_2O + K^+, (d) **9**-K + MeOH → **10** + MeO^- + H_2O + K^+. All interatomic distances are reported in Å.

We stated above that the protonation reaction **2** + H^+ → **4** is thermodynamically more favorable by 1.0 kcal/mol compared with the reaction of **2** with CO_2. This result should be consistent regardless of the reference energy of the proton (i.e., the pK_a of the Brønsted acid used in this reaction). However, the *barrier* for protonation of **2** is +10.1 kcal/mol larger than the barrier for the **2** + CO_2 → **7** pathway when MeOH is used as the Brønsted acid. Thus, this process is kinetically unfavorable. Note that the pK_a of MeOH in acetonitrile itself is quite high (calculated pK_a ≈ 37), and a K^+ counterion was needed to stabilize the highly unstable MeO^- conjugate base and prevent it from forming a chemical bond to the bpy ligand after deprotonation. In the presence of stronger Brønsted acids, protonation barriers would likely decrease since the conjugate base would be more stable. In the presence of HCl (calculated pK_a ≈ 11), we calculate the **2** + H^+ → **4** process to be barrierless, indicating that a threshold Brønsted acidity will change the mechanism of this process to favor H_2 formation. Indeed, the use of acids such as ammonium (experimental pK_a ≈ 16.5) leads to H_2 formation instead of CO_2 reduction.[46]

Species such as **7** are known to be isolable and relatively stable in solution, although they decompose over the course of minutes to hours to form species such as $[Re(bpy\text{-}R)(CO)_4]^+$ (**8**) and further reaction products.[10] Thus, once complex **7** is formed it could be protonated again by a Brønsted acid to form **8** and H_2O. Protonating **7** is downhill in energy (again, referenced to the energy of a free proton in acetonitrile), but the barrier for this process is +24.4 kcal/mol and required the presence of the K^+ counterion to stabilize the resulting MeO^- conjugate anion so that it does not immediately bind to the Re complex after the proton-transfer step. Having this coupled protonation and C−O bond breaking step occurring while the Re−C bond is maintained is reasonable in light of our calculations that show that removing $COOH^-$ from **7** to form $[Re(bpy)(CO)_3]^+$ is thermodynamically uphill by 53.9 kcal/mol, therefore disfavoring product formation via a dissociative mechanism.

Alternatively, one can also consider **7** undergoing a one-electron reduction at the electrode to form $[Re(bpy)(CO)_3(CO_2H)]^-$ (**9**) (see Figure 1e). This calculated redox potential is −1.47 V, which should be facile at the applied potentials needed to form complex **2**. We believe it is more probable that complex **9** protonates to form $[Re(bpy)(CO)_4]^0$ (**10**) + H_2O, since **9** should have a greater affinity to Brønsted

dx.doi.org/10.1021/ja406456g | J. Am. Chem. Soc. 2013, 135, 15823−15829

acids than does **7** by being more negatively charged. The barrier for this process is slightly lower, +22.5 kcal/mol, and including K^+ in our model was also necessary to stabilize the resulting MeO^- conjugate anion. The transition states we characterized for breaking the C−OH bond in **7** and **9** are substantially different: the interatomic C−O bond distances are 2.71 and 2.42 Å, respectively (see Figure 2c,d), showing that the protonation of **9** involves a significantly earlier transition state than protonation of **7**. Lastly, we note that these transition states also differ by the position of the K^+ with respect to the other molecular species. In **7**, the K^+ prefers to interact with multiple oxygen lone pairs within the transition state (Figure 2c). Geometry optimizations of the transition state describing protonation of **9** started from nuclear coordinates of the transition state found for protonation of **7**. Upon adding the additional electron to the system, the K^+ migrated in order to reside close to the oxygen lone pair of the MeO^- conjugate anion (Figure 2d). As expected, and as was the case involving intermediate **7**, removing $COOH^-$ directly from complex **9** to form $[Re(bpy)(CO)_3]^0$ brings a sizable thermodynamic energy penalty, 27.7 kcal/mol, making it unlikely that decomposition of **9** follows a dissociative mechanism. Instead, product formation likely requires the presence of a Brønsted acid to associate with **9** to catalyze C−O bond breaking.

Protonating **9** leads to **10** + H_2O. **10** is likely a highly transient species since it has not been observed spectroscopically from the reduction of **8** + e^- → **10** (calculated = −1.13 V, experiment = −1.15 V[47]). Indeed, the CO binding energy to **8** is 24.1 kcal/mol, while to **10** it is 8.8 kcal/mol. The one-electron reduction of **10** + e^- results in an unstable anion, $[Re(bpy)(CO)_4]^-$, which spontaneously decomposes to **2** + CO (calculated = −1.53 V). Since this potential is less negative than that for **3** + e^- → **2** + Cl^-, this process should be considered facile, and **10** can be considered highly transient and omitted from mechanistic discussions at potentials applied in these experiments.

Figure 3 presents a complete picture of the mechanisms depicted in Scheme 2, schematically displaying electrochemical reaction energetics at different applied potentials. Figure 3 shows that regardless of applied potential (and assuming the stepwise proton and electron transfer processes follow the same reaction path preference as vibronically active proton-coupled electron transfer),[48] the **2** + CO_2 + H^+ → **7** process has a lower barrier than the **2** + H^+ → **4** process when using methanol as the Brønsted acid. This potential independence of the relative barrier heights is because neither reaction path involves an electron transfer. Stronger Brønsted acids provide needed protons to facilitate CO_2 reduction, but stronger Brønsted acids also more effectively stabilize the transition state for the **2** + H^+ → **4** process, rendering it less selective for CO_2 reduction. Thus, an optimal catalyst for CO_2 reduction will require balancing these two factors. The figure also shows that the potential at which the reaction is electrocatalytic is −1.74 V, which is the potential at which the electrochemical energetics of each intermediate state denoted by the relevant complexes (**1** → **3** → **2** → **6** → **7** → **9** → **2** + H_2O + CO) is sequentially downhill in energy. In addition, once potentials become more negative than approximately −1.25 V (not shown in Figure 3), there is a crossover point where the **7** + H^+ → **8** pathway is no longer preferred, and the **7** + e^- → **9** and **9** + H^+ → **10** pathways are energetically favored. Finally, and perhaps most significantly, we can also see that under catalytic conditions (i.e., at −1.74 V), the protonation of complex **9** is the rate-determining step.

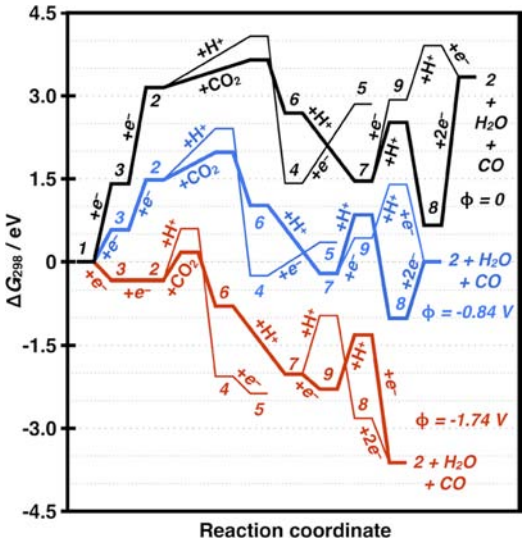

Figure 3. A mechanistic summary depicting overall reaction free energies and their dependencies on applied electrode potential. Numbers represent Re complexes shown in Scheme 2. Energetically preferred pathways at each potential are denoted with the thick lines.

Using Figure 3, one can now develop a blueprint for new generations of efficient CO_2 reduction catalysts. Ideally, different electrocatalysts would be identified with the following characteristics. (1) The electrocatalyst must form a species with a similar delocalized electronic structure as complex **2** so that it favors the CO_2-bound adduct that leads to CO_2 reduction and not hydrogen formation. (2) The first and second reduction potentials should be less negative than those for the Re complex so that less negative applied potentials are needed to reach the crucial intermediate analogous to **2**. (3) Catalysts must be developed with metals and ligands that destabilize intermediates **7** and **8** with respect to the energy of intermediate **2**, so that all reaction intermediates on the CO_2 reduction pathway have sequentially lower energies at a moderate applied potential. With steps 1−3 accomplished, the last requirement would be to tune catalysts to minimize barriers on the CO_2-reduction pathway so as to maximize reaction kinetics. By requiring less negative applied potentials, one is also opening the possibility of using semiconductor materials to generate electrical potentials from sunlight to drive the catalysis without a significant applied potential.

For a closing comment, we briefly mention that the *tert*-butyl substituted catalyst displays higher activities but also requires a more negative potential.[14] Further experimental work is needed to determine whether a species with electron-withdrawing groups on the bpy or other groups that electronically or electrostatically alter the environment around the complex can be used to achieve CO_2 reduction in the presence of acids at less negative potentials.

■ CONCLUSIONS

We have elucidated the mechanism of the proton-dependent two-electron pathway for reduction of CO_2 to CO by $Re(bpy)(CO)_3Cl$. After benchmarking accurate one-electron standard reduction potentials against experiment, we find that by decomposing the thermodynamics of individual proton- and electron-transfer processes, we can succinctly rationalize the

dx.doi.org/10.1021/ja406456g | J. Am. Chem. Soc. 2013, 135, 15823−15829

selectivity, proton dependence, and high efficiency of this catalyst. Selectivity toward CO_2 reduction is governed by reaction kinetics, while reaction thermodynamics would otherwise likely favor H_2 formation. Furthermore, the energetically preferred mechanism at experimentally applied potentials has complex **2** adding CO_2, then a proton, then an electron, at which point a Brønsted acid must associate with complex **9** to catalyze rate-determining C−O bond breaking. Current computational efforts are directed at understanding the effects of various proton donors on catalysis as well as the effect of installing *tert*-butyl and other groups in the 4,4′ positions of the bpy ligand. Catalysts based on earth-abundant manganese have been recently reported,[49,50] and studies are underway to examine the mechanisms for these catalysts as well.

■ ASSOCIATED CONTENT

Supporting Information

Details of computational methods and *xyz* coordinates of optimized geometries. This material is available free of charge via the Internet at http://pubs.acs.org.

■ AUTHOR INFORMATION

Corresponding Author

eac@princeton.edu

Author Contributions

The manuscript was written through contributions of all authors. All authors have given approval to the final version of the manuscript.

Notes

The authors declare no competing financial interest.

■ ACKNOWLEDGMENTS

We thank Dr. Christoph Riplinger for helpful discussions. This work was supported by the Air Force Office of Scientific Research through the MURI program (AFOSR Award No. FA9550-10-1-0572).

■ REFERENCES

(1) Concepcion, J. J.; House, R. L.; Papanikolas, J. M.; Meyer, T. J. *Proc. Natl. Acad. Sci. U. S. A.* **2012**, *109*, 15560−15564.

(2) Appel, A. M.; Bercaw, J. E.; Bocarsly, A. B.; Dobbek, H.; DuBois, D. L.; Dupuis, M.; Ferry, J. G.; Fujita, E.; Hille, R.; Kenis, P. J. A.; Kerfeld, C. A.; Morris, R. H.; Peden, C. H. F.; Portis, A. R.; Ragsdale, S. W.; Rauchfuss, T. B.; Reek, J. N. H.; Seefeldt, L. C.; Thauer, R. K.; Waldrop, G. L. *Chem. Rev.* **2013**, *113*, 6621−6658.

(3) Benson, E. E.; Kubiak, C. P.; Sathrum, A. J.; Smieja, J. M. *Chem. Soc. Rev.* **2009**, *38*, 89−99.

(4) Costentin, C.; Robert, M.; Savéant, J.-M. *Chem. Soc. Rev.* **2013**, *42*, 2423−2436.

(5) Windle, C. D.; Perutz, R. N. *Coord. Chem. Rev.* **2012**, *256*, 2562−2570.

(6) Kumar, B.; Llorente, M.; Froehlich, J.; Dang, T.; Sathrum, A.; Kubiak, C. P. *Annu. Rev. Phys. Chem.* **2012**, *63*, 541−569.

(7) Hawecker, J.; Lehn, J.-M.; Ziessel, R. *J. Chem. Soc., Chem. Commun.* **1984**, 328−330.

(8) Sullivan, B. P.; Bolinger, C. M.; Conrad, D.; Vining, W. J.; Meyer, T. J. *J. Chem. Soc., Chem. Commun.* **1985**, 1414−1416.

(9) Morris, A. J.; Meyer, G. J.; Fujita, E. *Acc. Chem. Res.* **2009**, *42*, 1983−1994.

(10) Agarwal, J.; Sanders, B. C.; Fujita, E.; Schaefer, H. F., III; Harrop, T. C.; Muckerman, J. T. *Chem. Commun.* **2012**, *48*, 6797−6799.

(11) Hawecker, J.; Lehn, J.-M.; Ziessel, R. *J. Chem. Soc., Chem. Commun.* **1983**, 536−538.

(12) Kumar, B.; Smieja, J. M.; Kubiak, C. P. *J. Phys. Chem. C* **2010**, *114*, 14220−14223.

(13) Smieja, J. M.; Benson, E. E.; Kumar, B.; Grice, K. A.; Seu, C. S.; Miller, A. J. M.; Mayer, J. M.; Kubiak, C. P. *Proc. Natl. Acad. Sci. U. S. A.* **2012**, 15646−15650.

(14) Smieja, J. M.; Kubiak, C. P. *Inorg. Chem.* **2010**, *49*, 9283−9289.

(15) Wong, K.-Y.; Chung, W.-H.; Lau, C.-P. *J. Electroanal. Chem.* **1998**, *453*, 161−169.

(16) Benson, E. E.; Kubiak, C. P. *Chem. Commun.* **2012**, *48*, 7374−7376.

(17) Benson, E. E.; Grice, K. A.; Smieja, J. M.; Kubiak, C. P. *Polyhedron* **2013**, 229−233.

(18) Benson, E. E.; Sampson, M. D.; Grice, K. A.; Smieja, J. M.; Froehlich, J. D.; Friebel, D.; Keith, J. A.; Carter, E. A.; Nilsson, A.; Kubiak, C. P. *Angew. Chem., Int. Ed.* **2013**, *52*, 4841−4844.

(19) Horvath, S.; Fernandez, L. E.; Appel, A. M.; Hammes-Schiffer, S. *Inorg. Chem.* **2013**, *52*, 3643−3652.

(20) Muckerman, J. T.; Fujita, E. *Chem. Commun.* **2011**, *47*, 12456−12458.

(21) Keith, J. A.; Carter, E. A. *J. Am. Chem. Soc.* **2012**, *134*, 7580−7583.

(22) Keith, J. A.; Carter, E. A. *Chem. Sci.* **2013**, *4*, 1490−1496.

(23) Lim, C.-H.; Holder, A. M.; Musgrave, C. B. *J. Am. Chem. Soc.* **2013**, *135*, 142−154.

(24) Ertem, M. Z.; Konezny, S. J.; Araujo, C. M.; Batista, V. S. *J. Phys. Chem. Lett.* **2013**, *4*, 745−748.

(25) Barton, E. E.; Rampulla, D. M.; Bocarsly, A. B. *J. Am. Chem. Soc.* **2008**, *130*, 6342−6344.

(26) Seshadri, G.; Lin, C.; Bocarsly, A. B. *J. Electroanal. Chem.* **1994**, *372*, 145−150.

(27) Becke, A. D. *Phys. Rev. A* **1988**, *38*, 3098−3100.

(28) Lee, C.; Yang, W.; Parr, R. G. *Phys. Rev. B* **1988**, *37*, 785−789.

(29) Gordon, M. S.; Schmidt, M. W. In *Theory and Applications of Computational Chemistry: The First Forty Years*; Dykstra, C., Frenking, G., Kim, K., Scuseria, G., Eds.; Elsevier Science: Amsterdam, 2005; pp 1167−1189.

(30) Schmidt, M. W.; Baldridge, K. K.; Boatz, J. A.; Elbert, S. T.; Gordon, M. S.; Jensen, J. H.; Koseki, S.; Matsunaga, N.; Nguyen, K. A.; Su, S.; Windus, T. L.; Dupuis, M.; Montgomery, J. A., Jr. *J. Comput. Chem.* **1993**, *14*, 1347−1363.

(31) Clark, T.; Chandrasekhar, J.; Spitznagel, G. W.; Schleyer, P. V. R. *J. Comput. Chem.* **1983**, *4*, 294−301.

(32) Hariharan, P. C.; Pople, J. A. *Theor. Chim. Acta* **1973**, *28*, 213−222.

(33) Hay, P. J.; Wadt, W. R. *J. Chem. Phys.* **1985**, *82*, 270−283.

(34) Cramer, C. J. *Essentials of Computational Chemistry: Theories and Models*, 2nd ed.; John Wiley & Sons, Inc.: Hoboken, NJ, 2004.

(35) Dunning, T. H. *J. Chem. Phys.* **1989**, *90*, 1007−1023.

(36) Barone, V.; Cossi, M. *J. Phys. Chem. A* **1998**, *102*, 1995−2001.

(37) Keith, J. A.; Carter, E. A. *J. Chem. Theory Comput.* **2012**, *8*, 3187−3206.

(38) Kelly, C. P.; Cramer, C. J.; Truhlar, D. G. *J. Phys. Chem. B* **2007**, *111*, 408−422.

(39) Muckerman, J. T.; Skone, J. H.; Ning, M.; Wasada-Tsutsui, Y. *Biochim. Biophys. Acta* **2013**, *1827*, 882−891.

(40) Isse, A. A.; Gennaro, A. *J. Phys. Chem. B* **2010**, *114*, 7894−7899.

(41) Nørskov, J. K.; Rossmeisl, J.; Logadottir, A.; Lindqvist, L.; Kitchin, J. R.; Bligaard, T.; Jónsson, H. *J. Phys. Chem. B* **2004**, *108*, 17886−17892.

(42) Liao, P.; Keith, J. A.; Carter, E. A. *J. Am. Chem. Soc.* **2012**, *134*, 13296−13309.

(43) Fujita, E.; Muckerman, J. T. *Inorg. Chem.* **2004**, *43*, 7636−7647.

(44) Keith, J. A.; Grice, K. A.; Ritzmann, A. M.; Riplinger, C.; Kubiak, C. P.; Carter, E. A. 2013, manuscript in preparation.

(45) Humphrey, W.; Dalke, A.; Schulten, K. *J. Mol. Graphics* **1996**, *14*, 33−38.

(46) Hawecker, J.; Lehn, J.-M.; Ziessel, R. *Helv. Chim. Acta* **1986**, *69*, 1990−2012.

(47) Grice, K. A.; Gu, N. X.; Sampson, M. D.; Kubiak, C. P. *Dalton Trans.* **2013**, *42*, 8498−8503.
(48) Hammes-Schiffer, S. *Energy Environ. Sci.* **2012**, *5*, 7696−7703.
(49) Bourrez, M.; Molton, F.; Chardon-Noblat, S.; Deronzier, A. *Angew. Chem., Int. Ed.* **2011**, *50*, 9903−9906.
(50) Smieja, J. M.; Sampson, M. D.; Grice, K. A.; Benson, E. E.; Froehlich, J. D.; Kubiak, C. P. *Inorg. Chem.* **2013**, *52*, 2484−2491.